applied sciences

MDPI

Article

Assessment of Natural Radioactivity and Radiological Risks in River Sediments from Calabria (Southern Italy)

Francesco Caridi [1,*], Marcella Di Bella [2,3], Giuseppe Sabatino [1], Giovanna Belmusto [4], Maria Rita Fede [5], Davide Romano [1,2], Francesco Italiano [2] and Antonio Francesco Mottese [1]

1 Department of Mathematics and Informatics, Physics and Earth Sciences (MIFT), University of Messina, Viale F. Stagno d'Alcontres 31, 98166 Messina, Italy; gsabatino@unime.it (G.S.); davide.romano@unime.it (D.R.); amottese@unime.it (A.F.M.)
2 Istituto Nazionale di Geofisica e Vulcanologia (INGV), Sezione di Palermo, Via Ugo La Malfa 153, 90146 Palermo and Milazzo Office, Via dei Mille 46, 98057 Milazzo (ME), Italy; mdibella@unime.it (M.D.B.); francesco.italiano@ingv.it (F.I.)
3 Stazione Zoologica Anton Dohrn (SZN), Villa Comunale, 80121 Napoli, Italy
4 Environmental Protection Agency of Calabria, Italy (ARPACal), Department of Reggio Calabria, Via Troncovito SNC, 89135 Reggio Calabria, Italy; gbelmusto@arpacal.it
5 Department of Biomedical and Dental Sciences and Morphofunctional Imaging SASTAS Section, University of Messina, Viale Annunziata, 98168 Messina, Italy; f_mariarita@yahoo.it
* Correspondence: fcaridi@unime.it

Abstract: This study was developed to carry out a comprehensive radiological assessment of natural radioactivity for river sediment samples from Calabria, southern Italy, and to define a baseline background for the area on a radiation map. In the studied area, elevated levels of natural radionuclides are expected, due to the outcropping acidic intrusive and metamorphic rocks from which the radioactive elements derive. To identify and quantify the natural radioisotopes, ninety river sediment samples from nine selected coastal sampling points (ten samples for each point) were collected as representative of the Ionian and the Tyrrhenian coastline of Calabria. The samples were analyzed using a gamma ray spectrometer equipped with a high-purity germanium (HPGe) detector. The values of mean activity concentrations of ^{226}Ra, ^{232}Th and ^{40}K measured for the studied samples are (21.3 ± 6.3) Bq kg^{-1}, (30.3 ± 4.5) Bq kg^{-1} and (849 ± 79) Bq kg^{-1}, respectively. The calculated radiological hazard indices showed average values of 63 nGy h^{-1} (absorbed dose rate), 0.078 mSv y^{-1} (effective dose outdoors), 0.111 mSv y^{-1} (effective dose indoors), 63 Bq kg^{-1} (radium equivalent), 0.35 (H_{ex}), 0.41 (H_{in}), 0.50 (activity concentration index) and 458 μSv y^{-1} (Annual Gonadal Equivalent Dose, AGED). In order to delineate the spatial distribution of natural radionuclides on the radiological map and to identify the areas with low, medium and high radioactivity values, the Surfer 10 software was employed. Finally, the multivariate statistical analysis was performed to deduce the interdependency and any existing relationships between the radiological indices and the concentrations of the radionuclides. The results of this study, also compared with values of other locations of the Italian Peninsula characterized by similar local geological conditions, can be used as a baseline for future investigations about radioactivity background in the investigated area.

Keywords: natural radioactivity; river sediments; gamma spectroscopy; radiological risks; background radioactivity; multivariate statistics

Citation: Caridi, F.; Di Bella, M.; Sabatino, G.; Belmusto, G.; Fede, M.R.; Romano, D.; Italiano, F.; Mottese, A.F. Assessment of Natural Radioactivity and Radiological Risks in River Sediments from Calabria (Southern Italy). *Appl. Sci.* **2021**, *11*, 1729. https://doi.org/10.3390/app11041729

Academic Editor: Richard Kouzes

Received: 20 January 2021
Accepted: 11 February 2021
Published: 15 February 2021

1. Introduction

Radioactivity naturally occurs in the environment. Aside from the cosmic radiation which bombards the earth from the outside of the atmosphere, the predominant natural source of human exposure to radiation doses is due to the terrestrial radiation which includes radionuclides of ^{238}U, ^{232}Th, ^{235}U series and ^{40}K [1].

It is established that the abundance of these primordial radionuclides depends on the local environment's geology [2,3]. Moreover, natural and anthropogenic events such

as flooding, radionuclide uptake by plants and the use of fertilizers, usually provoke an alteration in the distribution of the abundance levels of the radionuclides in the environment [4–6].

Studies of natural radiation are needed to establish reference levels, especially in areas where the hazard of radioactive exposure may be higher due to the lithological features of the geological context.

In this framework, central and southern Calabria (Southern Italy) can be considered as "risky" areas, since granitoids and metamorphic rocks that represent sources of radionuclides widely outcrop along the Serre and the Aspromonte Massifs. Moreover, recent studies highlighted the presence of heavy minerals, such as monazite and zircons, in the Calabrian rocks [7], which might contain high amounts of radioactive U and Th.

In this study, fluvial deposits from nine different selected sites from the Ionian and Tyrrhenian coastline of Calabria were analyzed. River sediments, consisting of mineral particles with different size and chemical composition, are considered reliable long-term indicators of river pollution by radionuclides, because water pollution components are deposited in the sediments [8]. Major sources of natural radionuclides in sediments have different possible origins, like weathering and recycling by erosion of terrestrial minerals and rocks (igneous or metamorphic) containing ^{40}K and radionuclides of uranium and thorium radioactive series, and also rainfall and other depositional phenomena such as landslides and precipitations [9]. The main aim of this paper is to identify and quantify natural gamma-emitting radionuclides and to evaluate the radiological hazard effects [10]. For this purpose, High-Purity Germanium (HPGe) gamma spectrometry was used to measure the ^{226}Ra (in secular equilibrium with ^{238}U), ^{232}Th and ^{40}K activity concentration [11]. Statistical and radiological maps were produced in order to detect the relationship among values and to identify the most hazardous zone.

Moreover, since sandy natural materials were widely used in the field of civil construction, a series of radiological indices were calculated to evaluate the potential hazard connected with the building use of these materials.

2. Geological Setting

The investigated river sediments come from the Ionian and Tyrrhenian seaboard of the Calabrian coastline (Figure 1), and they derive from the dismantling of the Serre Massifs and Aspromonte due to erosion processes. These Massifs belong to the Calabria-Peloritani Orogen (CPO), which is the peri-Mediterranean orogenic Alpine nappe system that comprises the whole Calabria and the north-eastern sector of Sicily [12]. It includes the Sila and Catena Costiera Massifs in northern Calabria, the Serre and Aspromonte Massifs in central and southern Calabria and the Peloritani Mountains in Sicily [12].

The Serre Massif (Central Calabria) is characterized by outcrops of granitoids and Variscan metamorphic rocks. A thin early Mesozoic sedimentary cover is present only along the Ionian margin. According to recent studies [12–14], the Serre Massif represents a nearly complete continental crust section, which is divided into lower, middle and upper crustal portions. The lower one is composed of granulitic and migmatitic complexes, whereas the middle one is made up by late-Variscan acidic granitoid rocks, such as tonalites, granodiorites and granites. Conversely, the upper crustal portion consists of high- to low-grade metapelites (Mammola and Stilo-Pazzano complexes) [13,14].

The Aspromonte Massif (Calabria), together with the Peloritani Mountains (Sicily), constitutes the southern sector of the CPO (Calabria Peloritani Orogen). This Massif was generated by the juxtaposition of three different tectonic units. The Madonna di Polsi Unit is the lowermost unit and it is composed of greenschist to amphibolite facies metamorphic rocks showing only Alpine metamorphism. The higher-most unit is represented by the Stilo Unit, made up of phyllites, schists and paragneisses derived from the variscan metamorphism of Paleozoic sediments. The Aspromonte Unit, which is sandwiched between the Stilo and Madonna di Polsi Unit, exhibits high-grade metamorphites and late-variscan granitoids [12–14].

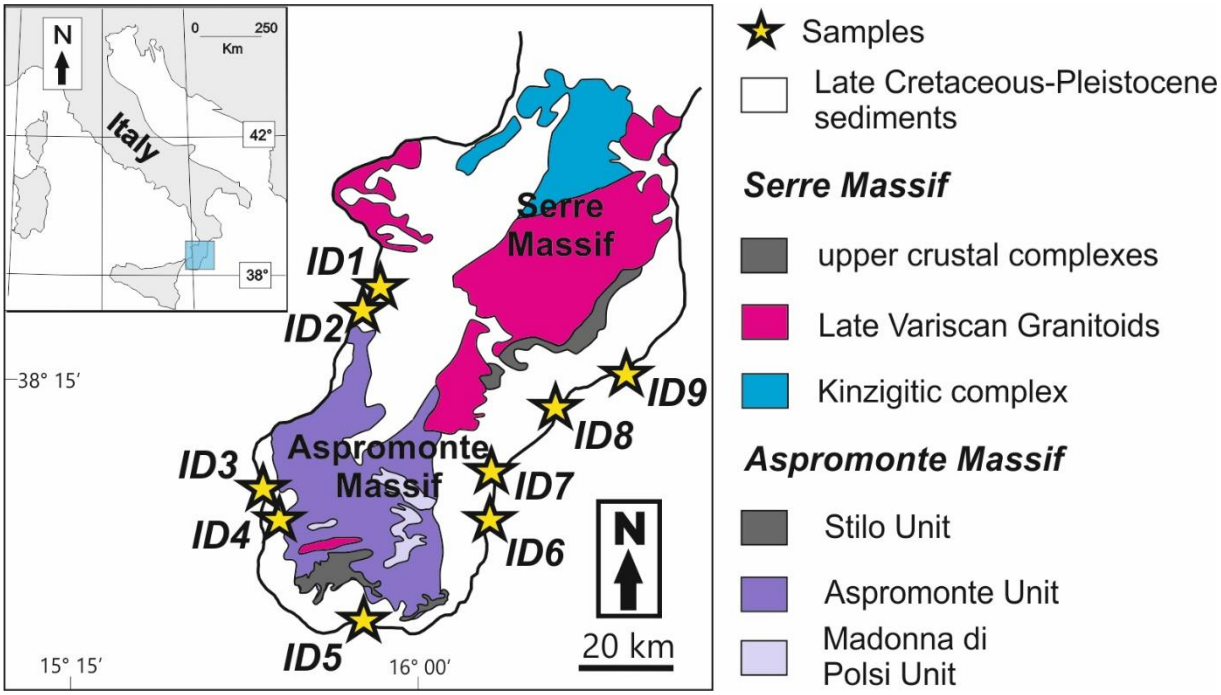

Figure 1. Geological sketch map of central-southern Calabria; yellow stars: sampling sites.

Paleozoic and early Mesozoic rocks of both Serre and Aspromonte Massif are covered by sedimentary deposits ranging in age from the Late Cretaceous to the Pleistocene.

3. Materials and Methods

3.1. Samples Collection and Preparation

Ninety samples of river sediments, around 1 kg each, were collected in nine selected sites of the Ionian and Tyrrhenian coast of Calabria for subsequent laboratory gamma spectrometric measurements. Locations, coordinates and labels of the collected samples are indicated in Figure 1 and in Table 1.

Table 1. Labels and Global Positioning System (GPS) locations of the sampling sites.

Site ID	Sampling Site	GPS Position	
		Latitude	Longitude
1	Gioia Tauro–Budello river	38.43	15.9075
2	Gioia Tauro–Petrace river	38.4202778	15.8839
3	Reggio Cal.–Gallico river	38.1730556	15.6506
4	Reggio Cal.–Calopinace river	38.1005556	15.6897
5	Bova Marina–Amendolea river	37.928333	15.8878
6	Africo–Laverde river	38.9291667	16.8338
7	Bovalivo–Bonamico river	38.1275	16.1591
8	Siderno–Novito river	38.2505556	16.2794
9	Caulonia–Allaro river	38.3480556	16.4727

Samples were collected with a metal sampler and stored in labeled plastic boxes. Adequate care was taken to prevent their contamination, particularly during transportation to the laboratory. Samples were oven-dried for 24 h at 110 °C until moisture was completely removed and constant mass was attained. They were grounded and further homogenized by passing them through a 2 mm sieve using a sieve shaker. After, they were successfully

inserted in Marinelli hermetically sealed containers of 1 L capacity. After 40 days, the secular radioactive equilibrium between ^{226}Ra and their daughter products was attained and samples were ready for gamma spectrometry counting.

3.2. Gamma Spectrometry Measurements

Specific activity measurements of the investigated samples were performed by using a high-purity germanium (HPGe) detector (Ortec, Oak Ridge, TN, USA) for gamma spectrometry analysis.

In order to reduce statistical uncertainty, samples were counted for 70,000 seconds and spectra were analyzed in order to obtain the activity concentration of ^{226}Ra, ^{232}Th and ^{40}K. The ^{226}Ra-specific activity was calculated through a weighted average of ^{214}Pb and ^{214}Bi (in secular equilibrium) specific activities. The ^{232}Th activity concentration was determined by using the 911.21 and 968.97 keV ^{228}Ac γ-ray lines; for ^{40}K, the evaluation was performed from its γ-line at 1460.8 keV. The experimental setup was composed by a positive biased Ortec HPGe detector (GEM) (Full Width at Half Maximum, FWHM) of 1:85 keV, peak to Compton ratio of 64:1, relative efficiency of 40% at the 1:33 MeV ^{60}Co-line), placed inside lead wells to shield the background radiation environment. Efficiency and energy calibrations were performed using a multipeak Marinelli geometry gamma source (AK-5901) of 1 L capacity, covering the energy range, 59.54–1836 keV, customized to reproduce the exact geometries of samples in a water-equivalent epoxy resin matrix [15].

The Gamma Vision (Ortec) software was used for data acquisition and analysis [16].

The activity concentration (Bq kg^{-1}) of the investigated radionuclides was calculated using the following formula [17]:

$$C = \frac{N_E}{\varepsilon_E t \gamma_d M} \quad (1)$$

where N_E indicates the net area of a peak at energy E, ε_E and γ_d are the efficiency and yield of the photopeak at energy E respectively, M is the mass of the sample (kg) and t is the live time (s).

The measurement uncertainty is a combined standard one at coverage factor k = 2, taking into account the following components: uncertainty counting statistics, uncertainty in nuclear data library, uncertainty due to calibration efficiency and uncertainty about the quantity of the sample [18].

The quality of the gamma spectrometry experimental results was certified by the Italian Accreditation Body (ACCREDIA) [19]. This implies the continued verification (with annual periodicity) of the maintenance of the gamma spectrometry method performance characteristics.

In particular, with regard to the blanks, they are generally determined by acquiring an empty lead well spectrum or an ultrapure water sample in the sample holder of the desired geometry (for determination of natural-emitting gamma radionuclides) or, in the case of samples requiring a material of support (e.g., atmospheric particulate aspirated on filter), by acquiring the support of clean sampling, under the same geometric conditions as the sample. The measurement of the blanks is performed on a quarterly basis.

Regarding the precision and accuracy assessment, we proceed as follows:

For the precision, with the double test method, the repeatability of the method is verified over time. A certified reference material (also containing the radionuclides K-40, Ra-226 and Th-232) is analyzed twice, with the activity concentration of the radionuclide of interest defined as X_1 (first measurement) and X_2 (second measurement). The probability level p = 0.95 is considered. The following formula is applied:

$$|x_1 - x_2| \leq \sqrt{2} \cdot s_r \cdot t \quad (2)$$

where t is the Student variable and s_r is the standard deviation of repeatability obtained in the validation phase.

For the accuracy, it is evaluated by comparing the reference (certified sample) and the measured values of the radionuclide of interest, taking into account the uncertainty. This is done using the u-test, with the following acceptability criterion:

$$u_{test} = \frac{\text{measured} - \text{reference}}{\sqrt{u_{meas}^2 - u_{ref}^2}} \leq 2 \quad (3)$$

where $u_{meas}{}^2$ and $u_{ref}{}^2$ are the uncertainties of the measured and reference values, respectively.

3.3. Radiological Indices

3.3.1. Absorbed Gamma Dose Rate

The absorbed gamma dose rate calculation is the first major step to evaluate the health risk [20]. It was estimated as follows [21]:

$$D\ (nGy{\cdot}h^{-1}) = 0.462{\cdot}C_{Ra} + 0.604{\cdot}C_{Th} + 0.0417{\cdot}C_K \quad (4)$$

where C_{Ra}, C_{Th} and C_K are the mean activity concentrations (Bq kg^{-1}) of ^{226}Ra, ^{232}Th and ^{40}K in the river sediments, respectively.

3.3.2. The Annual Effective Dose Equivalent

Annual estimated average effective dose equivalent (AEDE) received by an individual was calculated using the following equations with an outdoor occupancy of 20% and 80% for indoors [22]:

$$\text{AEDE (outdoor)}\ (mSv{\cdot}y^{-1}) = \text{absorbed dose}\ (nGy{\cdot}h^{-1}) \times 8760{\cdot}h \times 0.7{\cdot}Sv{\cdot}Gy^{-1} \times 0.2 \times 10^{-6} \quad (5)$$

$$\text{AEDE (indoor)}\ (mSv{\cdot}y^{-1}) = \text{absorbed dose}\ (nGy{\cdot}h^{-1}) \times 8760{\cdot}h \times 0.7{\cdot}Sv{\cdot}Gy^{-1} \times 0.8 \times 10^{-6} \quad (6)$$

3.3.3. Radium Equivalent Activity

The activity concentrations of the radionuclides measured in the analyzed samples do not give a direct measure of the γ-radiation dose incurred by the population. To estimate the gamma radiation dose due to activity concentrations of ^{226}Ra, ^{232}Th and ^{40}K in the river samples, especially when used as components of building construction, the radium equivalent activity is regularly utilized.

It is an index which describes the activities of ^{226}Ra, ^{232}Th and ^{40}Kin a single activity term. The gamma energy doses from these radionuclides in river sediments are different even if they are present in the same amount. Radium equivalent activity (Ra_{eq}) estimated in Bq kg^{-1} is evaluated with conditions that 1 Bq kg^{-1} of ^{226}Ra or 1.43 Bq kg^{-1} of ^{232}Th or 0.077 Bq kg^{-1} of ^{40}K produce equal gamma dose rate.

The radium equivalent activity was calculated as [23]:

$$Ra_{eq}\ (Bq{\cdot}kg^{-1}) = C_{Ra} + 1.43\ C_{Th} + 0.077{\cdot}C_K \quad (7)$$

3.3.4. Hazard Indices

External and internal radiation hazard indices were defined to limit the radiation dose to 1 mSv y^{-1} [24].

The external hazard index (H_{ex}) was calculated using the given equation:

$$H_{ex} = (C_{Ra}/370 + C_{Th}/259 + C_K/4810) \leq 1 \quad (8)$$

It must be lower than the unity for the radiation hazard to be negligible.

The internal hazard index (H_{in}) gives the internal exposure to carcinogenic radon and its short-lived progeny and it is given by the following formula:

$$H_{in} = (C_{Ra}/185 + C_{Th}/259 + C_K/4810) \leq 1 \quad (9)$$

3.3.5. Activity Concentration Index

Another radiation hazard, called the activity concentration index (I), has been defined by the European Commission [25] and it is given below:

$$I = (C_{Ra}/300 + C_{Th}/200 + C_K/3000) \quad (10)$$

The activity concentration index is correlated with the annual dose rate due to the excess external gamma radiation caused by superficial material. Values of $I \leq 1$ correspond to a criterion of 1 mSv y^{-1} [25]. Thus, this index should be used only as a screening tool to identify materials that might be of concern to be used as construction materials [26].

3.3.6. Annual Gonadal Equivalent Dose (AGED)

Some organs exhibit high sensitivity to radiation as they are highly susceptible to harmful effects of radiation. The gonads, the active bone marrow and the bone surface cells are considered to be the organs of importance due to their high radiosensitivity. The annual gonadal equivalent dose (AGED) due to the specific activities of ^{226}Ra, ^{232}Th and ^{40}K is evaluated using the following formula [27]:

$$AGED\ (\mu Sv \cdot y^{-1}) = 3.09 \cdot C_{Ra} + 4.18 \cdot C_{Th} + 0.314 \cdot C_K \quad (11)$$

where C_{Ra}, C_{Th} and C_K are the mean activity concentrations of ^{226}Ra, ^{232}Th and ^{40}K, respectively.

3.4. Delineation of Radiological Map

Surfer 10 software was employed to generate a radiological map for the study area [28]. The software uses the kriging interpolation method, used in geostatistics to predict the value of a random variable over a spatial region. Using the values of radiological measurements at all the sampling sites with different geographic coordinates, kriging allows the prediction of the radiological values throughout the regions where there are no experimental observations in the entire study area.

This method is widely employed in hydrogeology and environmental science, among others.

3.5. Statistical Analysis

The XLSTAT statistical software for Windows was used for all statistical calculations [29].

With the aim to individuate the presence of the relationships among the original variables (Pearson correlation analysis), an exploratory method (Principal Component Analysis, PCA) was performed. The PCA elaboration ensures the reduction of the data dimensionality, whereas the combinations of variables identified by the PCs provide the greatest contribution to sample variability. However, before the elaboration, the logarithmic transformation of the dataset was conducted and the appropriateness of the dataset was preliminarily checked by the Kaiser–Meyer–Olkin (KMO) test and the Bartlett test (sphericity test), as already reported in our previous work [30].

4. Results and Discussion

4.1. 226. Ra, ^{232}Th and ^{40}K Activity Concentration in the River Sediments, Spatial Distribution and Classification of Hazard Regions

The activity concentrations of the three naturally occurring ^{226}Ra, ^{232}Th and ^{40}K radionuclides in river sediments across the study area were determined for the sampling points reported in Table 1.

The obtained results are reported in Table 2. As shown in the Table, the highest average concentration, (31.3 ± 8.3) Bq kg^{-1}, of ^{226}Ra was obtained for samples from the site ID8 (Siderno–Novito river), whereas the lowest mean value, (14.5 ± 4.9) Bq kg^{-1}, was detected for sediments from the site ID1 (Gioia Tauro–Budello river). Concerning ^{232}Th, samples from the site ID8 are characterized by the highest average concentration, (43.5 ± 4.9) Bq kg^{-1}, while those from the site ID2 (Gioia Tauro–Petrace river) have the lowest mean value, (20.3 ± 2.9) Bq kg^{-1}. Sediments from the site ID1 show the highest average concentration of ^{40}K, with (1088 ± 98) Bq kg^{-1}, while the lowest mean concentration of (643 ± 53) Bq kg^{-1} was obtained for samples from the site ID 6 (Africo–Laverde river).

Table 2. Activity concentrations of ^{226}Ra, ^{232}Th and ^{40}K in the investigated sampling sites.

Scheme 226.	No. of Samples	^{226}Ra (Bq kg^{-1})		^{232}Th (Bq kg^{-1})		^{40}K (Bq kg^{-1})	
		Range	Mean	Range	Mean	Range	Mean
1	10	10.2–23.6	14.5 ± 4.9	16.5–48.6	22.7 ± 3.2	961–1450	1088 ± 98
2	10	13.6–22.9	18.2 ± 4.4	17.5–23.8	20.3 ± 2.9	949–1028	1009 ± 88
3	10	15.1–19.6	16.2 ± 4.3	37.2–41.5	39.5 ± 4.8	712–918	815 ± 77
4	10	15.1–18.8	16.5 ± 6.8	22.5–26.3	24.1 ± 2.9	591–811	722 ± 84
5	10	19.1–21.7	20.6 ± 2.3	20.3–46.8	27.8 ± 3.9	678–762	702 ± 66
6	10	19.3–29.4	26.2 ± 7.5	25.1–36.5	32.5 ± 9.2	528–691	643 ± 53
7	10	23.6–31.8	26.5 ± 9.5	28.2–43.5	34.5 ± 5.6	608–749	715 ± 60
8	10	26.6–33.9	31.3 ± 8.3	38.2–48.6	43.5 ± 4.9	871–942	917 ± 86
9	10	17.8–26.8	21.9 ± 8.5	25.3–33.8	27.7 ± 3.4	1002–1079	1030 ± 98
Overall	90	10.2–33.9	21.3 ± 6.3	16.5–48.6	30.3 ± 4.5	528–1450	849 ± 79

Across all sampling locations, the activity concentration values of ^{226}Ra ranged between 10.2 and 33.9 Bq kg^{-1}, with overall mean value of 21.3 ± 6.3 Bq kg^{-1}, that of ^{232}Th varied from 16.5 to 48.6 Bq kg^{-1} and the overall average value is (30.3 ± 4.5) Bq kg^{-1}. The ^{40}K ranged between 528 and 1450 Bq kg^{-1}, with an overall average value of (849 ± 79) Bq kg^{-1}.

The average values of ^{226}Ra, ^{232}Th and ^{40}K obtained in this study, for each sampling site, were compared with the world average value reported in Reference [1]. All the average values of ^{226}Ra are lower than that of the world average (35 Bq kg^{-1}). For ^{232}Th, the mean values are lower than that of the world average (30 Bq kg^{-1}) except for samples from the sites ID3 (39.5 ± 4.8 Bq kg^{-1}), ID6 (32.5 ± 9.2 Bq kg^{-1}), ID7 (34.5 ± 5.6 Bq kg^{-1}) and ID8 (43.5 ± 4.9 Bq kg^{-1}). The average concentration of ^{40}K is higher than the 420 Bq/kg average concentration reported in Reference [1] for all the analyzed samples.

Contour maps, showing the spatial distributions of ^{226}Ra, ^{232}Th and ^{40}K, are presented in Figure 2.

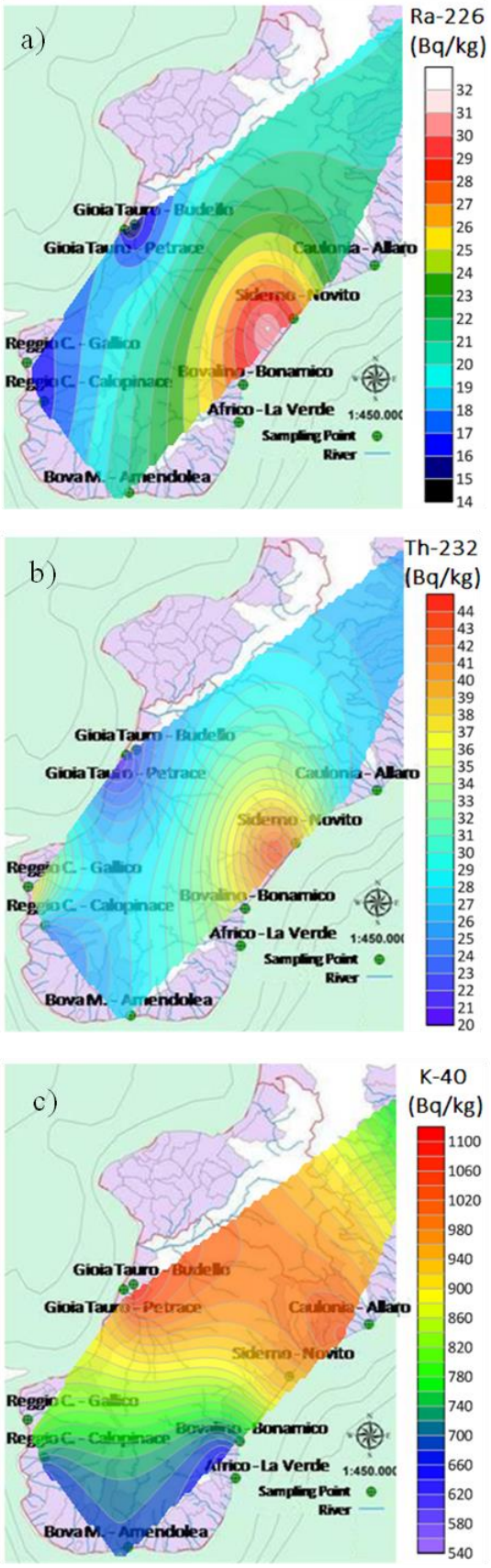

Figure 2. Contour maps showing the spatial distributions of (**a**) ^{226}Ra, (**b**) ^{232}Th and (**c**) ^{40}K in the investigated region.

As can be seen in the ^{226}Ra map (Figure 2a), there are four distinct regions. The activity concentration of ^{226}Ra in these regions was classified as low (C_{Ra} < 15 Bq kg^{-1}), moderate (15 Bq kg^{-1} < C_{Ra} < 20 Bq kg^{-1}), high (20 Bq kg^{-1} < C_{Ra} < 25 Bq kg^{-1}) and very high (C_{Ra} > 25 Bq kg^{-1}), which are deep blue, light blue, green and yellow (and red) areas on the map. In the case of ^{232}Th, two regions of very low and moderately low activity concentrations were identified. As seen from Figure 2b, the southern part of the study area as well as the mid-west and the northern part exhibit low activity concentrations of ^{232}Th with typical activities concentrations less than 33 Bq kg^{-1}. Otherwise, the middle-east zone of the study area exhibits high activity, higher than 35 Bq kg^{-1}. The delineated map of ^{40}K (Figure 2c) shows two distinct zones of concentration. The blue zone in the southern part belongs to the low-concentration region (lower than 700 Bq kg^{-1}). Whereas, other areas are classified as high-concentration zones (higher than 700 Bq kg^{-1}).

4.2. Dose Assessment and Hazard Indices

Table 3 reports the calculated average values of adsorbed and effective doses together with the hazard indices. The absorbed gamma dose rate was estimated using Equation (4). Measured values range from 52 to 79 nGy h^{-1}, with an average value of 63 nGy h^{-1}. This average value is near the world mean value of 60 nGy/h [1], although 66% of the analyzed samples showed values that are in excess than the world mean. The variability of the adsorbed and effective doses is attributable to the different lithologic components of the considered areas.

Table 3. Radiological indices in the investigated sampling sites.

Scheme 1.	Absorbed Dose Rate (nGyh^{-1})	Effective Dose Outdoors (mSv y^{-1})	Effective Dose Indoors (mSv y^{-1})	Ra_{eq} (Bq kg^{-1})	H_{ex}	H_{in}	I	Annual Gonadal Equivalent Dose (AGED) (μSvy^{-1})
1	66	0.081	0.323	66	0.35	0.39	0.52	481
2	63	0.077	0.084	63	0.33	0.39	0.50	457
3	66	0.080	0.088	65	0.36	0.41	0.52	471
4	52	0.064	0.070	52	0.28	0.33	0.42	378
5	56	0.068	0.075	55	0.30	0.36	0.44	400
6	58	0.072	0.079	58	0.33	0.40	0.46	418
7	63	0.077	0.085	63	0.35	0.43	0.50	450
8	79	0.097	0.106	79	0.44	0.53	0.63	566
9	70	0.086	0.094	69	0.38	0.44	0.55	506
Mean	63	0.078	0.111	63	0.35	0.41	0.50	458

Equation (5) was used to evaluate the annual outdoor effective dose due to the activities of ^{226}Ra, ^{232}Th and ^{40}K in the analyzed samples. The obtained values range from 0.064 to 0.097 mSv y^{-1}, with an average value of 0.078 mSv y^{-1}. In a similar way, the annual indoor effective dose (Equation (6)) ranges from 0.070 to 0.323 mSv y^{-1}, with a mean value of 0.111 mSv y^{-1}. The total average annual effective dose is therefore of 0.189 mSv y^{-1}. This value is lower than the worldwide average of annual effective dose (0.48 mSv y^{-1} [1]). The mean value is also lower than 1 mSv y^{-1}, which is set as the maximum limit by Reference [31].

The radium equivalent activity (Ra_{eq}) was calculated using Equation (7) in order to determine the suitability of the samples when they are used as components in building materials. The obtained Ra_{eq} values vary from 52 to 79 Bq kg^{-1} with an average value of 63 Bq kg^{-1}, which is lower than 370 Bq kg^{-1} set as the upper limit for building materials [29]. This indicates that the investigated samples may not be hazardous if used in the field of civil construction. The minimum value of radium equivalent activity was obtained

for the river sediments come from the site ID4 (Reggio Cal.–Calopinace river), while the maximum one characterizes the samples collected at the site ID8 (Siderno–Novito river).

The external and internal hazard indices, given by Equations (8) and (9), are lower than the unity for all investigated samples, thus the radiological risks can be considered negligible.

The activity concentration index, calculated with Equation (10), is again lower than the unity for all analyzed samples. Thus, these river sediments are not be of concern to be used as construction materials.

The obtained values of annual gonadal equivalent dose (AGED), calculated by Equation (11), range from 378 (site ID4) to 566 μSv y^{-1} (site ID8), with an average of 458 μSv y^{-1}, for the investigated samples. These values are higher than the world average value for AGED, for sediments, which in the literature was found to be 300 μSv y^{-1} [32].

4.3. Statistical Features

The radiological parameters obtained from the measured activity concentrations of ^{40}K, ^{226}Ra and ^{232}Th were subjected to Pearson's correlation analysis, with the aim to deduce the interdependency and identify any existing relationships between the radiological indices and the concentrations of the radionuclides. This will help in making valid assessments concerning the nature and distribution of these radionuclides in the study area. The results of the Pearson's correlation coefficients are presented in Table 4. Among the negative correlations, the most interesting are those between ^{40}K and ^{226}Ra (−0.287) and between ^{40}K and ^{232}Th (−0.305), while a perfect positive correlation is found between absorbed dose rate and effective dose outdoors (1.00), and between Ra_{eq} and absorbed dose rate (1.00) and effective dose outdoors (1.00). The correlations of the three radionuclides are positive and in agreement with all the radiological parameters considered in this study at $p < 0.01$, except for correlations between ^{226}Ra and H_{in} (0.739) and between ^{232}Th and H_{in} (0.719), obtained at $p < 0.05$.

Table 4. Pearson correlation matrix among the considered variables.

Pearson Correlation Matrix (n).											
Variables	**^{226}Ra**	**^{232}Th**	**^{40}K**	**Absorbed Dose Rate (nGy h^{-1})**	**Effective Dose Outdoors (mSv y^{-1})**	**Effective Dose Indoors (mSv y^{-1})**	**Ra_{eq} (Bq kg^{-1})**	**H_{ex}**	**H_{in}**	**Gamma index I**	**AGED μSv y^{-1}**
^{226}Ra	1	0.649	−0.287	0.468	0.465	−0.378	0.468	0.559	0.739	0.464	0.417
^{232}Th	0.649	1	−0.305	0.546	0.536	−0.281	0.546	0.666	0.719	0.553	0.494
^{40}K	−0.287	−0.305	1	0.595	0.603	0.607	0.596	0.465	0.301	0.591	0.647
Absorbed Dose Rate (nGy/h)	0.468	0.546	0.595	1	1.000	0.236	1.000	0.988	0.936	0.999	0.998
Effective Dose outdoors (mSv/y)	0.465	0.536	0.603	1.000	1	0.245	1.000	0.986	0.933	0.998	0.998
Effective Dose indoors (mSv/y)	−0.378	−0.281	0.607	0.236	0.245	1	0.237	0.148	0.002	0.223	0.275
Ra_{eq} (Bq/kg)	0.468	0.546	0.596	1.000	1.000	0.237	1	0.988	0.936	0.999	0.998
H_{ex}	0.559	0.666	0.465	0.988	0.986	0.148	0.988	1	0.970	0.988	0.976
H_{in}	0.739	0.719	0.301	0.936	0.933	0.002	0.936	0.970	1	0.935	0.912
Gamma index I	0.464	0.553	0.591	0.999	0.998	0.223	0.999	0.988	0.935	1	0.996
AGDE (μSv/y)	0.417	0.494	0.647	0.998	0.998	0.275	0.998	0.976	0.912	0.996	1

Bold values refer to $p < 0.05$.

Moreover, ^{226}Ra and ^{232}Th are negatively correlated with the annual effective dose equivalent indoors (−0.378 and −0.281, respectively). The radiological parameters are positively and significantly correlated with each other, showing direct relationships.

In order to better define the relationships among the specific activities of ^{226}Ra, ^{232}Th and ^{40}K, the PCA multivariate statistical method was carried out. The geological feature of sediments is the most important variable, neglecting the others (erosive power of

rivers, solid transport, selective erosion, weathering, etc.), which is useful to evaluate the degree of relationship between the isotopic specific activities and the samples' geolocation. Results of the PCA allow to group the sampling sites in four clusters that seem to be comparable to each other (Figure 3) in terms of activity concentration of ^{226}Ra, ^{232}Th and ^{40}K. Specifically, sites ID1 and ID2 show positive correlations with ^{40}K-specific activity but negative linear relationships with ^{226}Ra and ^{232}Th ones, whereas sites IDs 3, 4 and 5 are negatively correlated to the activity concentrations of ^{226}Ra, ^{232}Th and ^{40}K. The sites ID6 and ID7 show instead a positive correlation with values of ^{226}Ra- and ^{232}Th-specific activities, and exhibit a negative correlation with ^{40}K. Finally, sites ID8 and ID9 show positive correlations of the three investigated radionuclides' activity concentrations. We believe that the differences of ^{226}Ra-, ^{232}Th- and ^{40}K-specific activities among the identified clusters mainly depend on the compositional/mineralogical features of rocks from which the analyzed river sediments derive. The sediments collected along the rivers located in the Tyrrhenian side (ID1 and ID2) record the chemical fingerprint of the granitoid rocks from the Serre Massif. On the contrary, the Ionian river sediments (ID6, ID7, ID8 and ID9) reflect the chemical and mineralogical composition of the outcropping Late Cretaceous and Cenozoic terrigeous sediments. Moreover, the ID6 and ID7 rivers are characterized by a component provided by the erosion of the Aspromonte Unit, whereas clasts from the upper crustal complexes (Stilo-Pazzano and Mammola) and from granitoids supply the ID8 and ID9 rivers. Regarding the rivers on the western and southern margin of the Aspromonte Massif (ID3, ID4 and ID5), the main lithologies occurring within the drainage basins come from the Aspromonte and the Stilo Units.

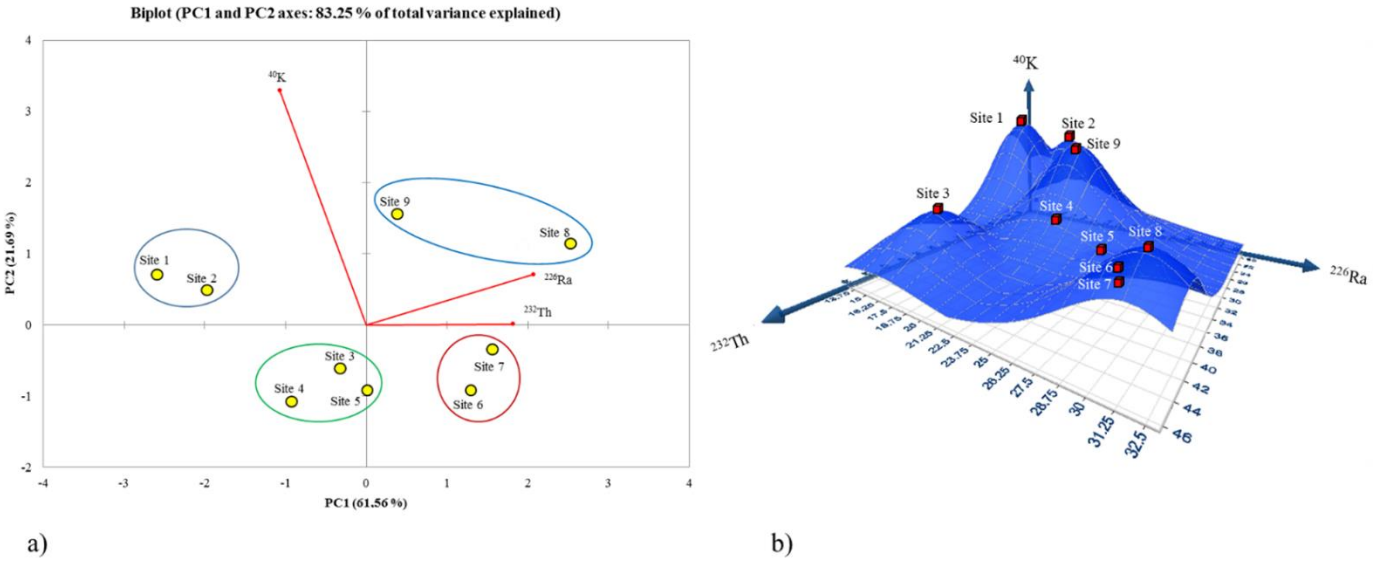

Figure 3. Two-dimensional (2D) plots of the first two Principal Components (PCs) obtained through Principal Component Analysis (PCA) elaboration starting from ^{40}K, ^{232}Th and ^{226}Ra activity concentrations (**a**). Mean concentration three-dimensional (3D) map of ^{40}K, ^{232}Th and ^{226}Ra into the investigated sites (**b**).

5. Conclusions

The activity concentration and the distribution of natural terrestrial radionuclides ^{226}Ra, ^{232}Th and ^{40}K for river sediments from selected locations of the Calabrian coastline (Southern Italy) were measured using HPGe gamma spectrometry. The obtained average values of the absorbed dose rate in air, AEDE (outdoor and indoor), Ra_{eq}, H_{ex} and H_{in}, I and AGDE are comparable with average worldwide ranges and they fell within the maximum recommended values.

The background radiation maps for the study area evidence that the Tyrrhenian side shows, in general, the lowest activity concentrations of ^{226}Ra and ^{232}Th, whereas the Ionian zone is characterized by the highest ones. Concerning the ^{40}K, an increasing of the

specific activity was defined from south to north. Multivariate statistical analysis allowed to assess the nature and distribution of natural radionuclides in the investigated area and highlighted the relationships between chemical/mineralogical features of the local outcropping lithologies.

Data provided in this study will serve to contribute as a reference database for future researches in the area, and also as a pilot scheme to provide a comprehensive background radiation map for Italy, which is not yet available.

Author Contributions: Conceptualization, F.C.; methodology, F.C. and A.F.M.; validation, F.C. and G.S.; formal analysis, F.C.; investigation, F.C., A.F.M., G.S., M.D.B., M.R.F., D.R. and F.I.; resources, G.S. and G.B.; data curation, F.C. and A.F.M.; writing—original draft preparation, F.C.; supervision, G.B. All authors have read and agreed to the published version of the manuscript.

Funding: This research received no external funding.

Institutional Review Board Statement: Not applicable.

Informed Consent Statement: Not applicable.

Conflicts of Interest: The authors declare no conflict of interest.

References

1. United Nations Scientific Committee on the Effects of Atomic Radiation (UNSCEAR). *Sources and Effects of Ionizing Radiation. Report of the United Nations Scientific Committee on the Effects of Atomic Radiation to the General Assembly*; United Nations: New York, NY, USA, 2000.
2. Baeza, A.; Del Rio, M.; Jimenez, A.; Miro, C.; Paniagua, J. Influence of geology and soil particle size on the surface-area/volume activity ratio for natural radionuclides. *J. Radioanal. Nucl. Chem.* **1995**, *189*, 289–299. [CrossRef]
3. Tzortzis, M.; Tsertos, H.; Christofides, S.; Christodoulides, G. Gamma-ray measurements of naturally occurring radioactive samples from Cyprus characteristic geological rocks. *Radiat. Meas.* **2003**, *37*, 221–229. [CrossRef]
4. Navas, A.; Soto, J.; Machin, J. Edaphic and physiographic factors affecting the distribution of natural gamma-emitting radionuclides in the soils of the Arnas catchment in the Central Spanish Pyrenees. *Eur. J. Soil Sci.* **2002**, *53*, 629–638. [CrossRef]
5. Pulhani, V.A.; Dafauti, S.; Heqde, A.G.; Sharma, R.M.; Mishra, U.C. Uptake and distribution of natural radioactivity in wheat plants from soil. *J. Environ. Radioact.* **2005**, *79*, 331–346. [CrossRef]
6. Chandrajith, R.; Seneviratna, S.; Wickramaarachchi, K.; Attanayake, T.; Aturaliya, T.N.C.; Dissanayake, C.B. Natural radionuclides and trace elements in rice field soils in relation to fertilizer application: Study of a chronic kidney disease area in Sri Lanka. *Environ. Earth Sci.* **2010**, *60*, 193–201. [CrossRef]
7. Fornelli, A.; Piccarreta, G.; Del Moro, A.; Acquafredda, P. Multi-stage melting in the lower crust of the Serre (southern Italy). *J. Petr.* **2002**, *43*, 2191. [CrossRef]
8. Sabatino, G.; Di Bella, M.; Caridi, F.; Italiano, F.; Romano, D.; Magazù, S.; Gnisci, A.; Faggio, G.; Messina, G.; Santangelo, S.; et al. Radiological assessment, mineralogy and geochemistry of the heavy-mineral placers from the Calabrian coast (South Italy). *J. Instrum.* **2019**, *14*, P05015. [CrossRef]
9. El-Gamal, A.; Nasr, S.; El-Taher, A. Study of the spatial distribution of natural radioactivity in the upper Egypt Nile river sediments. *Radiat. Meas.* **2007**, *42*, 457–465. [CrossRef]
10. Caridi, F.; Marguccio, S.; Belvedere, A.; D'Agostino, M.; Belmusto, G. A methodological approach to a radioactive sample analysis with low-level γ-ray spectrometry. *J. Instrum.* **2018**, *13*, P09022. [CrossRef]
11. Caridi, F.; Marguccio, S.; Belvedere, A.; D'Agostino, M.; Belmusto, G.; Durante, G.; Trozzo, R.; Fullone, F. Natural radioactivity measurements and dosimetric evaluations in soil samples with a high content of NORM. *Eur. Phys. J. Plus* **2017**, *132*, 56. [CrossRef]
12. Cirrincione, R.; Fazio, E.; Fiannacca, P.; Ortolano, G.; Pezzino, A.; Punturo, R. The Calabria-Peloritani Orogen, a composite terrane in Central Mediterranean; Its overall architecture and geodynamic significance for a pre-Alpine scenario around the Tethyan basin. *Periodico di Mineralogia* **2015**, *84*, 701–749. [CrossRef]
13. Caggianelli, A.; Liotta, D.; Prosser, G.; Ranalli, G. Pressure-temperature evolution of the late Hercyian Calabria continental crust: Compatibility with post-collisional extensional tectonics. *Terra Nova* **2007**, *19*, 502. [CrossRef]
14. Angì, G.; Cirrincione, R.; Fazio, E.; Fiannacca, P.; Ortolano, G.; Pezzino, A. Metamorphic evolution of preserved Hercynian crustal section in the Serre massif (Calabria-Peloritani Orogen, southern Italy). *Lithos* **2010**, *115*, 237. [CrossRef]
15. Caridi, F.; D'Agostino, M.; Belvedere, A.; Marguccio, S.; Belmusto, G.; Gatto, M.F. Diagnostics techniques and dosimetric evaluations for environmental radioactivity investigations. *J. Instrum.* **2016**, *11*, C10012. [CrossRef]
16. Caridi, F.; D'Agostino, M.; Messina, M.; Belvedere, A.; Marguccio, S.; Belmusto, G.; Marcianò, G.; Grioli, L. Lichens as environmental risk detectors. *Eur. Phys. J. Plus* **2017**, *132*, 189. [CrossRef]

17. Caridi, F.; Belvedere, A.; D'Agostino, M.; Marguccio, S.; Marino, G.; Messina, M.; Belmusto, G. An investigation on airborne particulate radioactivity, heavy metals and polycyclic aromatic hydrocarbons composition in Calabrian selected sites, southern Italy. *Ind. J. Environ. Protect.* **2019**, *39*, 321–326.
18. Caridi, F.; Messina, M.; Belvedere, A.; D'Agostino, M.; Marguccio, S.; Settineri, L.; Belmusto, G. Food salt characterization in terms of radioactivity and metals contamination. *Appl. Sci.* **2019**, *9*, 2882. [CrossRef]
19. Caridi, F.; D'Agostino, M.; Belvedere, A. Radioactivity in Calabrian (Southern Italy) wild boar meat. *Appl. Sci.* **2020**, *10*, 3580. [CrossRef]
20. Ramasamy, V.; Suresh, G.; Meenakshisundaram, V.; Ponnusamy, V. Horizontal and vertical characterization of radionuclides and minerals in river sediments. *Appl. Rad. Isot.* **2011**, *69*, 184–195. [CrossRef] [PubMed]
21. Caridi, F.; Pappaterra, D.; Belmusto, G.; Messina, M.; Belvedere, A.; D'Agostino, M.; Settineri, L. Radioactivity and heavy metals concentration in Italian (Calabrian) DOC wines. *Appl. Sci.* **2019**, *9*, 4584. [CrossRef]
22. Caridi, F.; Messina, M.; Faggio, G.; Santangelo, S.; Messina, G.; Belmusto, G. Radioactivity, radiological risk and metal pollution assessment in marine sediments from Calabrian selected areas, southern Italy. *Eur. Phys. J. Plus* **2018**, *133*, 65. [CrossRef]
23. Torrisi, L.; Visco, A.M.; Campo, N.; Caridi, F. Pulsed laser treatments of polyethylene films. *Nucl. Instrum. Methods Phys. Res. Sect. B Beam Interact. Mater. Atoms* **2010**, *268*, 3117–3121. [CrossRef]
24. Beretka, J.; Matthew, P.J. Natural radioactivity of Australian building materials, waste and by-products. *Health Phys.* **1985**, *48*, 87–95. [CrossRef]
25. Official Journal of the European Union. *Council Directive 2013/59/Euratom*; Official Journal of the European Union: Luxembourg, 2015.
26. Ravisankar, R.; Vanasundari, K.; Chandrasekaran, A.; Rajalakshmi, A.; Suganya, M.; Vijayagopal, P.; Meenakshisundaram, V. Measurement of natural radioactivity in building materials of Namakkal, Tamil Nadu, India using gamma-ray spectrometry. *Appl. Rad. And Isot.* **2012**, *70*, 699–704. [CrossRef] [PubMed]
27. Darwish, D.A.E.; Abul-Nasr, K.T.M.; El-Khayatt, A.M. The assessment of natural radioactivity and its associated radiological hazards and dose parameters in granite samples from South Sinai, Egypt. *J. Radiat. Res. Appl. Sci.* **2015**, *8*, 17–25. [CrossRef]
28. Surfer 10 Software. Available online: https://www.goldensoftware.com/products/surfer (accessed on 17 November 2020).
29. XLSTAT: Statistical Software & Data Analysis Add-On for Excel. Available online: https://www.xlstat.com/en/ (accessed on 16 November 2020).
30. Mottese, A.F.; Sabatino, G.; Di Bella, M.; Fede, M.R.; Caridi, F.; Parisi, F.; Marcianò, G.; Caccamo, M.T.; Italiano, F.; Yuce, G.; et al. Environmental screening for the assessment of potentially toxic elements content in PGI soils from the Mediterranean region (Italy and Turkey). *Environ. Earth Sci.* **2020**, *79*, 499. [CrossRef]
31. International Commission on Radiological Protection (ICRP). 1990 Recommendations of the International Commission on Radiological Protection. ICRP Publication 60. *Ann. ICRP* **1991**, *21*, 1–3.
32. Chandrasekaran, A.; Ravisankar, R.; Senthilkumar, G.; Thillaivelavan, K.; Dhinakaran, B.; Vijayagpal, P.; Bramha, S.N.; Venkatraman, B. Spatial distribution and lifetime cancer risk due to gamma radioactivity in Yelagiri Hills, Tamilnadu, India. *Egypt J. Basic Appl. Sci.* **2014**, *1*, 38–48. [CrossRef]